

DPVI: A Dynamic-Weight Particle-Based Variational Inference Framework

Chao Zhang¹, Zhijian Li^{2*}, Hui Qian¹, Xin Du^{2†}

¹College of Computer Science and Technology, Zhejiang University

²Information Science and Electronic Engineering, Zhejiang University
{zczju, lizhijian, qianhui, duxin}@zju.edu.cn

Abstract

The recently developed Particle-based Variational Inference (ParVI) methods drive the empirical distribution of a set of *fixed-weight* particles towards a given target distribution π by iteratively updating particles' positions. However, the fixed weight restriction greatly confines the empirical distribution's approximation ability, especially when the particle number is limited. In this paper, we propose to dynamically adjust particles' weights according to a Fisher-Rao reaction flow. We develop a general Dynamic-weight Particle-based Variational Inference (DPVI) framework according to a novel continuous composite flow, which evolves the positions and weights of particles simultaneously. We show that the mean-field limit of our composite flow is actually a Wasserstein-Fisher-Rao gradient flow of certain dissimilarity functional \mathcal{F} , which leads to a faster decrease of \mathcal{F} than the Wasserstein gradient flow underlying existing fixed-weight ParVIs. By using different finite-particle approximations in our general framework, we derive several efficient DPVI algorithms. The empirical results demonstrate the superiority of our derived DPVI algorithms over their fixed-weight counterparts.

1 Introduction

Recently, Particle-based Variational Inference (ParVI) methods have drawn much attention in the Bayesian inference literature, due to their success in efficiently approximating the target posterior distribution π (Liu and Wang 2016; Liu and Zhu 2018; Liu and Wang 2018; Pu et al. 2017; Zhu, Liu, and Zhu 2020). The core of ParVIs lies at evolving the empirical distribution of M *fixed-weight* particles by simulating a *continuity equation* through its easy-to-calculate finite-particle position transport approximation (Liu et al. 2019). Typically, the continuity equation is constructed according to the Wasserstein gradient flow of certain dissimilarity functional $\mathcal{F}(\mu) := \mathcal{D}(\mu|\pi)$ vanishing at $\mu = \pi$ (Liu et al. 2019). By using different dissimilarity functionals \mathcal{F} and position transport approximations, several ParVIs have been proposed, e.g., Stein Variational Gradient Descent (SVGD) method (Liu and Wang 2016), Blob¹ (Chen et al.

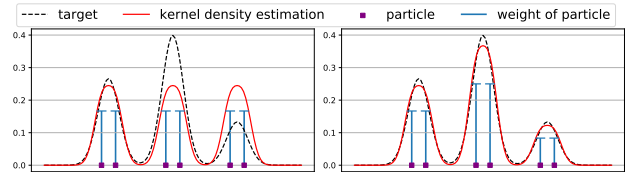


Figure 1: Approximating a Gaussian mixture distribution with six particles. The black dashed lines denote the target density, the solid red lines are the densities of particles (estimated using the kernel density estimator), and the heights of the solid blue lines represent the weight of each particle. The left sub-figure shows the result of the fixed-weight ParVI algorithm Blob, and the right sub-figure is from our dynamic-weight D-Blob-CA algorithm.

2018a), GFSD (Liu et al. 2019), the Kernel Stein Discrepancy Descent (KSDD) (Korba et al. 2021).

Fixed weight restriction. Existing ParVIs have a common fixed weight restriction, i.e., they all keep the particles' weights fixed during the whole procedure, and only update the positions of particles according to the position transport approximation derived from a continuity equation. This restriction severely confines the empirical distribution's approximation ability, especially when the particle number M is limited (depicted in Figure 1). To mitigate the influence of this restriction, existing ParVIs require plenty of particles to obtain satisfying approximation accuracy (Liu and Wang 2018; Korba et al. 2020). As a result, a large amount of computation is usually needed since the per-iteration computational cost in ParVIs is typically in the square order of M . Actually, a huge deviation between the empirical distribution and the target π is often observed when the particle number is insufficient due to a limited computational budget (Zhang et al. 2020; Zhang, Zhao, and Chen 2020).

Thus, it is in great need to find an effective weight adjustment strategy and design dynamic-weight ParVI algorithms which could achieve a high approximation accuracy with fewer particles and hence less computation. Note that, though the continuity equation underlying existing fixed-weight ParVIs can be directly transformed into an easy-to-calculate position transport approximation, adjusting weights according to the continuity equation is generally infeasible as the divergence operator in it would introduce great computational challenge. Constructing effective algo-

*Chao Zhang and Zhijian Li contribute equally.

†Contact Author.

Copyright © 2022, Association for the Advancement of Artificial Intelligence (www.aaai.org). All rights reserved.

¹This method is originally called w -SGLD-B. Here, we follow (Liu et al. 2019) and denote it as Blob.

gorithms to evolve a set of dynamic-weight particles towards the target π is still an open problem in the ParVI field.

To tackle this problem, we propose to dynamically adjust particles’ weights according to the Fisher-Rao reaction flow of the underlying functional \mathcal{F} , and design a continuous-time composite flow, which evolves the positions and weights of M particles simultaneously. Specifically, the composite flow is a combination of a finite-particle approximation of the reaction flow and a finite-particle position transport approximation of the continuity equation. Different dynamic-weight ParVI algorithms can be obtained by discretizing the continuous flow with different discretization schemes and dissimilarity functionals \mathcal{F} . The contribution of our paper are listed as follows:

- We show that the mean-field limit of our proposed composite flow is actually the gradient flow of \mathcal{F} in the Wasserstein-Fisher-Rao space, which leads to a faster decrease of \mathcal{F} compared with both the Wasserstein gradient flow underlying existing fixed-weight ParVI algorithms and the Fisher-Rao reaction flow.
- We propose a general Dynamic-weight Particle-based Variational Inference (DPVI) framework, which utilizes an Euler discretization of the composite flow and adopts a Gauss-Siedel-type strategy to update the positions and the weights. Note that the weight adjustment step can be implemented without bringing much extra computation compared to the position update step. By adopting different dissimilarity functionals \mathcal{F} in DPVI, we can obtain different efficient dynamic-weight ParVI algorithms.
- We propose three efficient DPVI algorithms by using different dissimilarity functionals \mathcal{F} and their associated finite-particle approximations in the general framework. Besides, we also derive three duplicate/kill variants of our proposed algorithms, where a probabilistic discretization to the weight adjustment part in the composite flow is used to dynamically duplicate/kill particles, instead of adjusting the particles’ weights continuously.

We evaluate our algorithms on various synthetic and real-world tasks. The empirical results demonstrate the superiority of our dynamic weight strategy over the fixed weight strategy, and our DPVI algorithms constantly outperform their fixed-weight counterparts in all the tasks.

Notation. Given a probability measure μ on \mathbb{R}^d , we denote $\mu \in \mathcal{P}_2(\mathbb{R}^d)$ if its second moment is finite. For a given functional $\mathcal{F}(\mu) : \mathcal{P}_2(\mathbb{R}^d) \rightarrow \mathbb{R}$, $\frac{\delta \mathcal{F}(\rho)}{\delta \rho} : \mathbb{R}^d \rightarrow \mathbb{R}$ denote its first variation at $\mu = \rho$. Besides, we use ∇ and $\nabla \cdot (\cdot)$ to denote the gradient and the divergence operator, respectively.

2 Preliminaries

2.1 Particle-Based Variational Inference Methods

When dealing with Bayesian inference tasks, classical Variational Inference methods approximate the target posterior π with an easy-to-sample distribution μ , and recast the inference task as an optimization problem over $\mathcal{P}_2(\mathbb{R}^d)$ (or its

subspace) (Ranganath, Gerrish, and Blei 2014):

$$\min_{\mu \in \mathcal{P}_2(\mathbb{R}^d)} \mathcal{F}(\mu) := \mathcal{D}(\mu|\pi). \quad (1)$$

To solve this optimization problem, one can consider a descent flow of $\mathcal{F}(\mu)$ in the Wasserstein space, which transports any initial distribution μ_0 towards the target distribution π (Wibisono 2018). Specifically, the descent flow of $\mathcal{F}(\mu)$ is described by the following *continuity equation* (Ambrosio, Gigli, and Savaré 2008; Santambrogio 2017):

$$\partial_t \mu_t = -\nabla \cdot (\mu_t \mathbf{v}_{\mu_t}), \quad (2)$$

where $\mathbf{v}_{\mu_t} : \mathbb{R}^d \rightarrow \mathbb{R}^d$ is a vector field that defines the direction of position transportation. To ensure a descent of $\mathcal{F}(\mu_t)$ over time t , the vector field \mathbf{v}_{μ_t} should satisfy the following inequality (Ambrosio, Gigli, and Savaré 2008):

$$\frac{d\mathcal{F}(\mu_t)}{dt} = \int \langle \nabla \frac{\delta \mathcal{F}(\mu_t)}{\delta \mu_t}, \mathbf{v}_{\mu_t} \rangle d\mu_t \leq 0. \quad (3)$$

A straightforward choice of \mathbf{v}_{μ_t} is $\mathbf{v}_{\mu_t} = -\nabla \frac{\delta \mathcal{F}(\mu_t)}{\delta \mu_t}$, which is actually the steepest descent direction of $\mathcal{F}(\mu_t)$. From now on, we fix this choice of \mathbf{v}_{μ_t} in (2). We note that the continuity equation (2) with this \mathbf{v}_{μ_t} is also known as the *Wasserstein gradient flow* of \mathcal{F} .

To simulate the Wasserstein gradient flow of \mathcal{F} , existing ParVIs evolve a set of M fixed-weight particles and use the empirical distribution $\tilde{\mu}_t = \sum_{i=1}^M a_t^i \delta_{\mathbf{x}_t^i}$ to approximate μ_t in (2), where \mathbf{x}_t^i and a_t^i (usually set to $1/M$) denote the position and the weight of the i -th particle at time t , respectively. Specifically, ParVIs update the position of each particle \mathbf{x}_t^i according to the following finite-particle *position transport approximation* of the continuity equation (2) (Chen et al. 2018a; Liu 2017; Craig and Bertozzi 2016):

$$d\mathbf{x}_t^i = \mathbf{v}_{\tilde{\mu}_t}(\mathbf{x}_t^i) dt, \quad (4)$$

where $\mathbf{v}_{\tilde{\mu}_t}$ is an approximation of \mathbf{v}_{μ_t} through the empirical distribution $\tilde{\mu}_t$. It can be verified that the empirical distribution $\tilde{\mu}_t$ weakly converges to μ_t defined in (2) when $M \rightarrow \infty$ under mild conditions (Korba et al. 2020; Liu 2017; Liu and Wang 2018). Therefore, one can obtain different ParVIs by choosing proper $\mathbf{v}_{\tilde{\mu}_t}$ and discretizing (4) with certain scheme (the first-order explicit Euler discretization is set as a default). Note that adjusting weight a_t^i according to the continuity equation (2) is difficult, as directly discretizing (2) needs to calculate the second-order derivative of the first variation due to the divergence operator. Hence, existing ParVIs only update the position \mathbf{x}_t^i and keep the weight a_t^i fixed during the whole procedure.

To develop a ParVI method, it remains to select a proper dissimilarity functional \mathcal{F} and construct an approximation $\mathbf{v}_{\tilde{\mu}_t}$ of the vector field \mathbf{v}_{μ_t} . From the seminal SVGD to the subsequent Blob and GFSD, KL-divergence is widely adopted as the underlying dissimilarity functional (Liu and Wang 2016; Chen and Zhang 2017; Chen et al. 2018a; Liu et al. 2019; Liu, Zhuo, and Zhu 2019; Zhang et al. 2020). The associated vector field is defined as follows (Jordan, Kinderlehrer, and Otto 1998; Liu et al. 2019):

$$\mathbf{v}_{\mu_t} = -\nabla \frac{\delta \text{KL}(\mu_t|\pi)}{\delta \mu_t} = -\nabla \log \frac{\mu_t}{\pi} = \nabla \log \pi - \nabla \log \mu_t.$$

As $\nabla \log \mu_t$ is undefined with the empirical distribution $\tilde{\mu}_t$, the KL-divergence based ParVIs use different approaches to construct suitable approximations to the vector field. In SVGD, Liu and Wang (2016) restrict the vector field \mathbf{v}_{μ_t} within the unit ball of a Reproducing Kernel Hilbert Space (RKHS), and propose to approximate \mathbf{v}_{μ_t} by

$$\mathbf{v}_{\tilde{\mu}_t}(\cdot) = \mathbb{E}_{\mathbf{x}' \sim \tilde{\mu}_t} [K(\mathbf{x}', \cdot) \log \pi(\mathbf{x}) + \nabla_{\mathbf{x}'} K(\mathbf{x}', \cdot)], \quad (5)$$

where K is a kernel function, such as the Radial Basis Function (RBF) kernel. Subsequently, Blob (Chen et al. 2018a) reformulates the intractable term $\nabla \log \mu_t$ by partly smoothing the density with a kernel function K : $\nabla \left(\frac{\delta}{\delta \tilde{\mu}_t} \mathbb{E}_{\tilde{\mu}_t} [\tilde{\mu}_t * K] \right)$, while GFSD (Liu et al. 2019) directly approximates μ_t by $\tilde{\mu}_t * K$, where $*$ denotes the convolution operator. Recently, Kernel Stein Discrepancy Descent (KSDD) (Korba et al. 2021) method considers the Kernel Stein Discrepancy (KSD) (Liu, Lee, and Jordan 2016) as the underlying functional \mathcal{F} , whose first variation is compatible with empirical distribution and can be calculated directly.

2.2 Fisher-Rao Distance and Reaction Flow

The Fisher-Rao distance (Rao 1945; Kakutani 1948) is a metric defined for general positive Radon measures and allows comparing measures with mass variations. For two probability measures $(\beta_0, \beta_1) \in \mathcal{P}_2(\mathbb{R}^d)$, if they have densities (ρ_0, ρ_1) w.r.t. the Lebesgue measure, their Fisher-Rao distance is defined as follows (Nikulin et al. 2001):

$$\text{FR}(\beta_0, \beta_1) = \|\sqrt{\rho_0} - \sqrt{\rho_1}\|_{L^2}.$$

The positive Radon measure space equipped with the Fisher-Rao distance is known as the Fisher-Rao space. For a given dissimilarity functional $\mathcal{F}(\mu)$, its gradient flow in the Fisher-Rao space, also named as the Fisher-Rao reaction flow (Gallouët, Laborde, and Monsaingeon 2019; Gallouët and Monsaingeon 2017), is described by the following equation (Wang and Li 2019; Liero, Mielke, and Savaré 2016):

$$\partial_t \mu_t = -\alpha_{\mu_t} \mu_t, \quad \alpha_{\mu_t} = \frac{\delta \mathcal{F}(\mu_t)}{\delta \mu_t} - \int \frac{\delta \mathcal{F}(\mu_t)}{\delta \mu_t} d\mu_t, \quad (6)$$

where $\alpha_{\mu_t} : \mathbb{R}^d \rightarrow \mathbb{R}$ represents a construction/destruction function of mass. Since the average variation of μ_t equals zero due to the extra integral term $\int \frac{\delta \mathcal{F}(\mu_t)}{\delta \mu_t} d\mu_t$, the total mass of μ_t is conserved during the whole procedure (Lu, Lu, and Nolen 2019; Rotskoff et al. 2019). The target distribution π is actually an invariant distribution of this flow, as the first variation of the dissimilarity functional \mathcal{F} vanishes at π , i.e., $\frac{\delta \mathcal{F}(\pi)}{\delta \pi} = 0$. It can be verified that with a proper \mathcal{F} , the process (6) starting from a given μ_0 evolves towards the target distribution π (Kondratyev et al. 2016).

For a fixed position \mathbf{x} , the process (6) provides an effective way to adjust its density (weight) $\mu_t(\mathbf{x})$ at each time t according to the function α_{μ_t} . Thus, given a set of weighted particles and its empirical distribution $\tilde{\mu}_t$, one can adjust the weight by discretizing the reaction flow with an empirical approximate construction/deconstruction function $\alpha_{\tilde{\mu}_t}$. Though the reaction flow has been adopted in particle-based methods in other literature, such as MCMC (Lu, Lu, and

Nolen 2019), global minimization (Rotskoff et al. 2019) and generative models (Mroueh and Rigotti 2020), to the best of our knowledge, it has never been adopted in the ParVI literature to adjust the weights of particles.

3 Methodology

In this section, we first construct a composite flow that evolves positions and weights of particles simultaneously and investigate its mean-field property. Then, we develop our DPVI framework by discretizing this composite flow. We finally provide three effective DPVI algorithms by using different dissimilarity functionals \mathcal{F} (KL-divergence and KSD) and finite-particle approximations. Besides, we also derive the duplicate/kill variants of our proposed algorithms.

3.1 Continuous-Time Composite Flow

Based on the position transport approximation (4) for displacing the position and the Fisher-Rao reaction flow (6) for adjusting weight in previous sections, we consider the following composite flow that evolves the positions \mathbf{x}^i 's and the weights a^i 's of M particles simultaneously.

$$\begin{cases} d\mathbf{x}_t^i = \mathbf{v}_{\tilde{\mu}_t} dt, \\ da_t^i = - \left(U_{\tilde{\mu}_t}(\mathbf{x}_t^i) - \sum_{i=1}^M a_t^i U_{\tilde{\mu}_t}(\mathbf{x}_t^i) \right) a_t^i dt, \\ \tilde{\mu}_t = \sum_{i=1}^M a_t^i \delta_{\mathbf{x}_t^i}. \end{cases} \quad (7)$$

For ease of notation, we use U_μ and \mathbf{v}_μ to denote the first variation of $\mathcal{F}(\mu)$ at μ and the vector field associated with it, respectively, i.e., $U_\mu = \frac{\delta \mathcal{F}(\mu)}{\delta \mu}$ and $\mathbf{v}_\mu = -\nabla U_\mu$. Although the mean-field limit of the empirical distribution with either the position update part $d\mathbf{x}_t^i$ or the weight adjustment part da_t^i alone has the target distribution π as its stationary distribution, the behaviour of the empirical distribution $\tilde{\mu}_t$ in (7) remains unknown. Thus, we first investigate the mean-field limit of $\tilde{\mu}_t$ and show that it actually follows the gradient flow of \mathcal{F} in the Wasserstein-Fisher-Rao space when $M \rightarrow \infty$. Due to limited space, we refer readers to the Appendix for detailed proof of all the propositions.

Proposition 1. *Suppose the empirical distribution $\tilde{\mu}_0^M$ of M weighted particles weakly converges to a distribution μ_0 when $M \rightarrow \infty$. Then, the path of (7) starting from $\tilde{\mu}_0^M$ weakly converges to a solution of the following partial differential equation starting from μ_0 as $M \rightarrow \infty$:*

$$\partial_t \mu_t = \nabla \cdot (\mu_t \nabla U_{\mu_t}) - \left(U_{\mu_t} - \int U_{\mu_t} d\mu_t \right) \mu_t, \quad (8)$$

which is actually the gradient flow of \mathcal{F} in the Wasserstein-Fisher-Rao space.

Compared to the Wasserstein gradient flow (2) of \mathcal{F} , the Wasserstein-Fisher-Rao gradient flow (8) has an additional density adjustment part (second term in the r.h.s. of equation (8)). It can be verified that (8) results in a faster decrease of \mathcal{F} than the Wasserstein gradient flow used in the fixed-weight ParVIs due to the additional density adjustment part.

Proposition 2. Consider the Wasserstein-Fisher-Rao gradient flow (8) of a given functional \mathcal{F} , the differentiation of $\mathcal{F}(\mu_t)$ with respect to the time t satisfies:

$$\frac{d\mathcal{F}(\mu_t)}{dt} = - \int \left\| \nabla \left(\frac{\delta\mathcal{F}(\mu_t)}{\delta\mu_t} \right) \right\|^2 d\mu_t \quad (9)$$

$$- \left(\int \left| \frac{\delta\mathcal{F}(\mu_t)}{\delta\mu_t} \right|^2 d\mu_t - \left(\int \frac{\delta\mathcal{F}(\mu_t)}{\delta\mu_t} d\mu_t \right)^2 \right).$$

Note that the first part on the r.h.s. of (9) comes from the position update dx_t^i and the second part is resulted from the weight adjustment da_t^i . As a result, it can be verified that the mean-field limit of the composite flow leads to a faster decrease of \mathcal{F} compared with either the Wasserstein gradient flow or the Fisher-Rao reaction flow of \mathcal{F} . With proper dissimilarity functional \mathcal{F} such as the KL-divergence, it can be further proved that the Wasserstein-Fisher-Rao gradient flow (8) evolves to the target π faster than both the Wasserstein gradient flow (2) and the Fisher-Rao reaction flow under mild conditions (Lu, Lu, and Nolen 2019). For a general dissimilarity \mathcal{F} , it remains an open problem that whether the extra density adjustment would result in a faster convergence to the target π , and we leave it as an interesting future work.

3.2 Dynamic-Weight ParVI Framework

Generally, it is impossible to obtain an analytic solution of the continuous composite flow (7), thus a numerical integration method is required to derive an approximate solution. Note that any numerical solver, such as the implicit Euler method (Platen and Bruti-Liberati 2010) and higher-order Runge-Kutta method (Butcher 1964) can be used. Here, we adopt the first-order explicit Euler discretization (Süli and Mayers 2003) since it is simple and easy-to-implement, and propose our Dynamic-weight Particle-based Variational Inference (DPVI) framework, as listed in Algorithm 1.

Starting from M weighted particles located at $\{\mathbf{x}_0^i\}_{i=1}^M$ with weights $\{a_0^i\}_{i=0}^M$, DPVI first updates the positions of particles according to the following rule:

$$\mathbf{x}_{k+1}^i = \mathbf{x}_k^i + \eta \mathbf{v}_{\tilde{\mu}_k}(\mathbf{x}_k^i), \quad (10)$$

where $\tilde{\mu}_k = \sum_{i=1}^M a_k^i \delta_{\mathbf{x}_k^i}$. Then, it adjusts the particles' weights following

$$a_{k+1}^i = a_k^i - \lambda \eta \bar{U}_{\tilde{\mu}_{k+1/2}}(\mathbf{x}_{k+1}^i) a_k^i, \quad (11)$$

where $\bar{U}_{\tilde{\mu}_{k+1/2}} = U_{\tilde{\mu}_{k+1/2}} - \sum_{i=1}^M a_k^i U_{\tilde{\mu}_{k+1/2}}(\mathbf{x}_{k+1}^i)$, and $\tilde{\mu}_{k+1/2} = \sum_{i=1}^M a_k^i \delta_{\mathbf{x}_{k+1}^i}$ represents the empirical distribution after the position update (10). Here, we assume that a suitable empirical approximation $U_{\tilde{\mu}_k}$ of the first variation is already constructed, and we will discuss this comprehensively in the following subsection. It can be verified that the total mass of $\tilde{\mu}_k$ is conserved as the following equality holds:

$$\sum_{i=1}^M \eta \bar{U}_{\tilde{\mu}_{k+1/2}}(\mathbf{x}_{k+1}^i) a_k^i = 0,$$

Thus, $\tilde{\mu}_k$ remains a valid probability distribution during the whole procedure of DPVI, i.e. $\sum_i a_k^i = 1$ for all k .

In developing our DPVI framework, we adopt a Gauss-Siedel-type strategy to update the position \mathbf{x}_k^i and the weight

Algorithm 1: Dynamic-weight Particle-based Variational Inference (DPVI) Framework

Input: Initial distribution $\tilde{\mu}_0 = \sum_{i=1}^M a_0^i \delta_{\mathbf{x}_0^i}$, step-size η , weight parameter λ .

- 1: **for** $k = 0, 1, \dots, T - 1$ **do**
 - 2: **for** $i = 1, 2, \dots, M$ **do**
 - 3: Update positions \mathbf{x}_{k+1}^i 's according to (10).
 - 4: **end for**
 - 5: **for** $i = 1, 2, \dots, M$ **do**
 - 6: Adjust weights a_{k+1}^i 's according to (11).
 - 7: **end for**
 - 8: **end for**
 - 9: **Output:** $\tilde{\mu}_T = \sum_{i=1}^M a_T^i \delta_{\mathbf{x}_T^i}$.
-

a_k^i , i.e., we adjust the weight based on the newly obtained position \mathbf{x}_{k+1}^i in the k -th iteration. As the weight adjustment step (11) only involves calculating the first variation approximation $U_{\tilde{\mu}_{k+1/2}}$, it would bring little extra computational cost compared with the position update step (10), which involves calculating the gradient of $U_{\tilde{\mu}_k}$. Besides, one can further reduce the computational cost by adopting the Jacobi-type strategy, i.e., update weight a_k^i in (11) with $U_{\tilde{\mu}_k}$ at position \mathbf{x}_k^i . In this case, the weight adjustment step boils down to M scalar additions since the term $U_{\tilde{\mu}_k}$ can be directly obtained when calculating $\mathbf{v}_{\tilde{\mu}_k} = -\nabla U_{\tilde{\mu}_k}$ in the position update step (10). Here, we adopt the Gauss-Siedel-type update strategy as it usually has better empirical performance without bringing much additional computational cost compared with the Jacobi-type update strategy.

3.3 DPVI algorithms and their duplicate/kill variants

To derive an efficient DPVI algorithm, it remains to decide the underlying functional \mathcal{F} , and construct proper empirical approximations to its first variation U_μ and the associated vector field $\mathbf{v}_\mu = -\nabla U_\mu$ (denoted as $U_{\tilde{\mu}}$ and $\mathbf{v}_{\tilde{\mu}}$, respectively). Unfortunately, there exists no systematic approach to design proper approximations $U_{\tilde{\mu}}$ and $\mathbf{v}_{\tilde{\mu}}$ for arbitrary dissimilarity functional \mathcal{F} . Here, we propose three efficient DPVI algorithms based on different approximations utilized in existing fixed-weight ParVIs, two with the KL-divergence as the underlying functional \mathcal{F} and one with the KSD.

KL-divergence as \mathcal{F} . As we have discussed in the preliminaries, a large portion of existing fixed-weight ParVIs adopt the KL-divergence as underlying functional \mathcal{F} , whose associated vector field and first variation are defined as follows:

$$\mathbf{v}_\mu(\mathbf{x}) = \nabla \log \pi(\mathbf{x}) - \nabla \log \mu(\mathbf{x}),$$

$$U_\mu(\mathbf{x}) = \log \mu(\mathbf{x}) - \log \pi(\mathbf{x}).$$

In order to deal with the intractable $\log \mu(\mathbf{x})$ which is undefined with empirical distribution $\tilde{\mu}_k$, we adopt the approximation techniques used in the fixed-weight ParVI methods GFSD (Liu et al. 2019) and Blob (Chen et al. 2018a), and derive two KL-divergence based DPVI algorithms.

D-GFSD-CA algorithm. Our first DPVI algorithm utilizes the same approximation technique in the fixed-weight GFSD

algorithm, and we name it as D-GFSD-CA algorithm (“CA” for *Continuous Adjustment*). Specifically, we directly approximate μ by smoothing the empirical distribution $\tilde{\mu}$ with a kernel function K : $\hat{\mu} = \tilde{\mu} * K = \sum_{i=1}^M a^i K(\cdot, \mathbf{x}^i)$, which leads to the following approximations:

$$\mathbf{v}_{\tilde{\mu}_k}(\mathbf{x}) = \nabla \log \pi(\mathbf{x}) - \frac{\sum_{i=1}^M a_k^i \nabla_{\mathbf{x}} K(\mathbf{x}, \mathbf{x}_k^i)}{\sum_{i=1}^M a_k^i K(\mathbf{x}, \mathbf{x}_k^i)}, \quad (12)$$

$$U_{\tilde{\mu}_{k+1/2}}(\mathbf{x}) = -\log \pi(\mathbf{x}) + \log \sum_{i=1}^M a_k^i K(\mathbf{x}, \mathbf{x}_{k+1}^i). \quad (13)$$

D-Blob-CA algorithm. We name our second DPVI algorithm as D-Blob-CA, which uses the same approximation technique adopted by the fixed-weight Blob method. In particular, we reformulate the intractable term $\log \mu$ from the perspective of its first variation $\frac{\delta}{\delta \mu} \mathbb{E}_{\mu} [\log \mu]$ and partly smooth the density with a kernel function K :

$$\begin{aligned} \frac{\delta}{\delta \tilde{\mu}} \mathbb{E}_{\tilde{\mu}} [\log (\tilde{\mu} * K)] &= \log (\tilde{\mu} * K) + \frac{\tilde{\mu}}{\tilde{\mu} * K} * K \\ &= \log \sum_{i=1}^M a^i K(\cdot, \mathbf{x}^i) + \sum_{i=1}^M \frac{a^i K(\cdot, \mathbf{x}^i)}{\sum_{l=1}^M a^l K(\mathbf{x}^i, \mathbf{x}^l)}. \end{aligned}$$

This leads to the following approximation results:

$$\begin{aligned} \mathbf{v}_{\tilde{\mu}_k}(\mathbf{x}) &= \nabla \log \pi(\mathbf{x}) - \frac{\sum_{i=1}^M a_k^i \nabla_{\mathbf{x}} K(\mathbf{x}, \mathbf{x}_k^i)}{\sum_{i=1}^M a_k^i K(\mathbf{x}, \mathbf{x}_k^i)} \\ &\quad - \sum_{i=1}^M \frac{a_k^i \nabla_{\mathbf{x}} K(\mathbf{x}, \mathbf{x}_k^i)}{\sum_{l=1}^M a_k^l K(\mathbf{x}_k^i, \mathbf{x}_k^l)}, \end{aligned} \quad (14)$$

$$\begin{aligned} U_{\tilde{\mu}_{k+1/2}}(\mathbf{x}) &= -\log \pi(\mathbf{x}) + \log \sum_{i=1}^M a_k^i K(\mathbf{x}, \mathbf{x}_{k+1}^i) \\ &\quad + \sum_{i=1}^M \frac{a_k^i K(\mathbf{x}, \mathbf{x}_{k+1}^i)}{\sum_{l=1}^M a_k^l K(\mathbf{x}_{k+1}^i, \mathbf{x}_{k+1}^l)}. \end{aligned} \quad (15)$$

Remark 1. *In the above approximations, we call the terms defined through the interaction with other particles as the repulsive terms. It can be observed that the Blob-type approximations (14) and (15) have an extra repulsive term (the term in the second line) compared to the GFSD-type approximations (12) and (13). Practically, this extra repulsive term would drive the particles away from each other further, and result in a better exploration of particles in the probability space. Actually, the Blob-type methods usually outperforms the GFSD-type methods empirically.*

Since GFSD and Blob (partly) smooth the original empirical distribution $\tilde{\mu}$ with a kernel function K , the underlying evolutionary distribution is actually a smoothed version of $\tilde{\mu}$. To update the positions and the weights in the smoothed empirical distribution, one should solve a system of linear equations to obtain the new positions \mathbf{x}_{k+1}^i ’s and weights a_{k+1}^i ’s in the k -th iteration. Nevertheless, with a proper kernel function K , such as the RBF kernel, the density $\mu(\mathbf{x}^i)$ at a given position \mathbf{x}^i mainly comes from its corresponding weight a^i . Hence, we can still update the positions and weights according to (10) and (11), respectively.

KSD as \mathcal{F} . Except for the KL-divergence, KSD is recently adopted as the dissimilarity functional in the fixed-weight ParVI method KSDD (Korba et al. 2021), whose first variation and the corresponding vector field are defined as

$$\begin{aligned} \mathbf{v}_{\mu}(\mathbf{x}) &= \mathbb{E}_{\mathbf{x}' \sim \mu} [\nabla_{\mathbf{x}} k_{\pi}(\mathbf{x}', \mathbf{x})], \\ U_{\mu}(\mathbf{x}) &= \mathbb{E}_{\mathbf{x}' \sim \mu} [k_{\pi}(\mathbf{x}', \mathbf{x})]. \end{aligned} \quad (16)$$

Here, k_{π} denotes the Stein kernel (Liu, Lee, and Jordan 2016), and it is defined by the score of π : $s(\mathbf{x}) = \nabla \log \pi(\mathbf{x})$ and a positive semi-definite kernel function K :

$$\begin{aligned} k_{\pi}(\mathbf{x}, \mathbf{y}) &= s(\mathbf{x})^T s(\mathbf{y}) K(\mathbf{x}, \mathbf{y}) + s(\mathbf{x})^T \nabla_{\mathbf{y}} K(\mathbf{x}, \mathbf{y}) \\ &\quad + \nabla_{\mathbf{x}} K(\mathbf{x}, \mathbf{y})^T s(\mathbf{y}) + \nabla_{\mathbf{x}} \cdot \nabla_{\mathbf{y}} K(\mathbf{x}, \mathbf{y}). \end{aligned}$$

D-KSDD-CA algorithm. The vector field \mathbf{v}_{μ} and the first variation U_{μ} in (16) can be directly approximated via the empirical distribution $\tilde{\mu}$. We construct the following finite-particle approximations $\mathbf{v}_{\tilde{\mu}_k}$ and $U_{\tilde{\mu}_{k+1/2}}$:

$$\begin{aligned} \mathbf{v}_{\tilde{\mu}_k}(\mathbf{x}) &= \sum_{i=1}^M a_k^i \nabla_{\mathbf{x}} k_{\pi}(\mathbf{x}_k^i, \mathbf{x}), \\ U_{\tilde{\mu}_{k+1/2}}(\mathbf{x}) &= \sum_{i=1}^M a_k^i k_{\pi}(\mathbf{x}_k^i, \mathbf{x}). \end{aligned}$$

By using with these approximations in DPVI, we obtain the D-KSDD-CA algorithm.

The duplicate/kill variants. In fact, there is a probabilistic discretization strategy of the approximate reaction flow in (7), which has been used by particle-based methods in other literature (Lu, Lu, and Nolen 2019; Rotskoff et al. 2019). This strategy duplicates/kills particle \mathbf{x}_{k+1}^i according to an exponential clock with instantaneous rate:

$$R_{k+1}^i = -\lambda \eta \bar{U}_{\tilde{\mu}_{k+1/2}}(\mathbf{x}_{k+1}^i). \quad (17)$$

Specifically, if $R_{k+1}^i > 0$, duplicate the particle \mathbf{x}_{k+1}^i with probability $1 - \exp(-R_{k+1}^i)$, and kill another one with uniform probability to conserve the total mass; if $R_{k+1}^i < 0$, kill the particle \mathbf{x}_{k+1}^i with probability $1 - \exp(R_{k+1}^i)$, and duplicate another one with uniform probability.

This Duplicate/Kill (DK) strategy could also be used as an alternative to the CA strategy (11) in the DPVI framework. By replacing CA with DK in D-GFSD-CA, D-Blob-CA and D-KSDD-CA, we derive three DPVI variants, denoted as D-GFSD-DK, D-Blob-DK and D-KSDD-DK, respectively. Note that due to the deterministic position update fashion of ParVI algorithms, the particles may collapse to few positions during this duplicate/kill procedure. Thus, we inject an additional Gaussian noise with variance scaled by step-size for the duplicated particle to avoid particle collapse.

The DK strategy has also been used in a dynamics based MCMC method, Birth Death Langevin Sampling (BDLS) (Lu, Lu, and Nolen 2019). Specifically, BDLS update M particles independently according to the Langevin dynamics, a special form of the Wasserstein gradient flow of the KL-divergence (Chen et al. 2018a), and use the DK strategy to duplicate/kill particles. Though both the dynamics based MCMC methods and the ParVIs are suitable for Bayesian inference, ParVIs are usually more particle-efficient as they use the repulsive force between particles to drive the particles away from each other and explore the whole space (Liu et al. 2019). Actually, we also observe that the performance of BDLS is worse than the KL-divergence based DPVI algorithms due to the lack of interaction between particles.

Algorithm	Number of particles				
	5	10	20	50	100
ULD	2.467	1.818	1.398	0.977	0.835
BDLS	2.549	1.694	1.368	0.974	0.746
SVGD	1.963	1.339	1.094	0.917	0.648
GFSD	2.044	1.489	1.292	1.080	0.902
D-GFSD-DK	1.791	1.306	1.129	0.791	0.693
D-GFSD-CA	1.618	1.096	0.884	0.642	0.496
Blob	1.970	1.390	1.150	0.888	0.596
D-Blob-DK	1.736	1.193	0.881	0.639	0.530
D-Blob-CA	1.532	1.014	0.763	0.516	0.388
KSDD	1.964	1.379	1.183	1.086	0.936
D-KSDD-DK	2.011	1.452	1.172	1.089	0.919
D-KSDD-CA	1.948	1.366	1.174	1.054	0.932

Table 1: W_2 distances with different number of particles.

4 Experiments

In this section, we conduct empirical studies with our DPVI algorithms (D-GFSD-CA, D-Blob-CA, and D-KSDD-CA), their duplicate/kill variants (D-GFSD-DK, D-Blob-DK, and D-KSDD-DK), and the fixed-weight ParVI algorithms (SVGD, GFSD, Blob and KSDD). Besides, we also include BDLS (Lu, Lu, and Nolen 2019) and the Unadjusted Langevin Dynamics (ULD) method (Ma, Chen, and Fox 2015) (the fixed-weight counterpart of BDLS) as our baselines. We compare the performance of these algorithms on two simulations, i.e., bivariate Gaussian model and Gaussian mixture model (GMM), and two real-world applications, i.e. Gaussian Process (GP) regression and Bayesian neural network. For all the algorithms, the particles’ weights are initialized to be equal. We repeat all the experiments 10 times and report the average results. Due to limited space, only parts of the results are reported in this section. We refer readers to the Appendix for the experiment on the bivariate Gaussian model and additional results for GMM.

4.1 Gaussian Mixture Model

We consider approximating a 2-D Gaussian mixture model with two components, weighted by $1/3$ and $2/3$ respectively. To investigate the influence of particle number M in fixed-weight ParVIs and the dynamic-weight algorithms, we run all the algorithms with $M \in \{5, 10, 20, 50, 100\}$.

In Table 1, we report the 2-Wasserstein (W_2) distance between the empirical distribution generated by each algorithm and the target distribution. We generate 2100 samples from the target distribution π as reference to evaluate the W_2 distance by using the POT library (Flamary et al. 2021). It can be observed that both the CA and DK weight strategies contribute to obtain a higher approximation accuracy, and CA usually results in better performance as it allows weights to vary in $[0, 1]$ continuously. The DPVI algorithms constantly outperform their fixed-weight counterparts with the same or even less number of particles. For instance, D-GFSD-CA with $M = 20$ achieves a lower W_2 than the fixed-weight GFSD algorithm with $M = 100$. Moreover, the results also show that, with a fixed particle number M , D-Blob-CA achieves the best performance among all the algorithms,

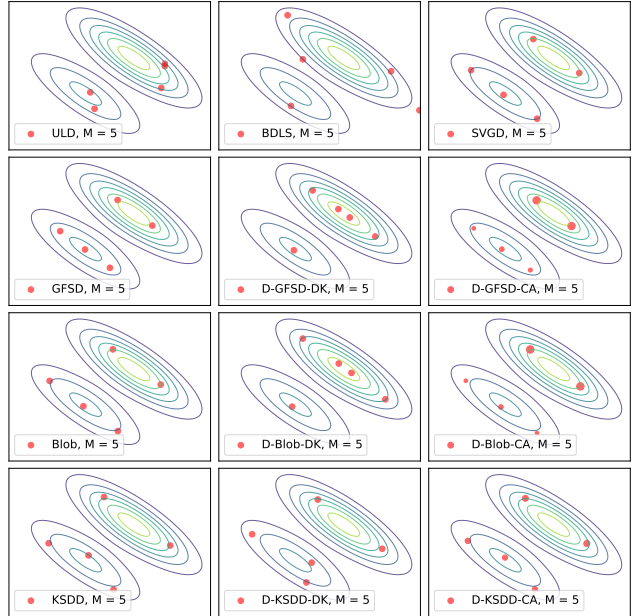


Figure 2: Results on approximating a Gaussian mixture distribution with 5 particles.

due to both the dynamic weight strategy and extra repulsive term. Besides, the KL-divergence based DPVIs outperform BDLS due to the particle efficiency of DPVI, as discussed in the last paragraph of Section 3.3. Note that the KSDD-type algorithms (KSDD, D-KSDD-CA, and D-KSDD-DK) perform poorly in this task. Actually, this phenomenon has already been reported in KSDD (Korba et al. 2021), and the authors claim that particles in KSDD may get stuck in spurious local minima when dealing with multi-mode models.

In Figure 2, we plot the output of each algorithm when $M = 5$, and the particle size is proportional to its weight. From this figure, we can observe that, compared with the fixed-weight ParVI algorithms, both the CA and DK strategies result in more mass of the empirical distribution on the larger component of the target distribution. Specifically, the DK strategy concentrates more particles on the larger component, due to its ability to duplicate particles with larger target probability densities; the CA strategy increases the weight of each particle on the larger component, though algorithms with CA strategy put less particles on this component. Actually, according to the results in the first column of Table 1, the DPVI algorithms with CA obtain higher approximation accuracy than their DK variants.

4.2 Gaussian Process Regression

The Gaussian Process (GP) model is widely adopted for the uncertainty quantification in regression problems (Rasmussen 2003). We follow the experiment setting in (Chen et al. 2018b), and use the dataset LIDAR (denoted as $\mathcal{D} = \{(x_i, y_i)\}_{i=1}^N$) which consists of 221 observations of scalar variable x_i and y_i . Denote $\mathbf{x} = [x_1, x_2, \dots, x_N]^T$ and $\mathbf{y} = [y_1, y_2, \dots, y_N]^T$, the target log-posterior w.r.t. the model pa-

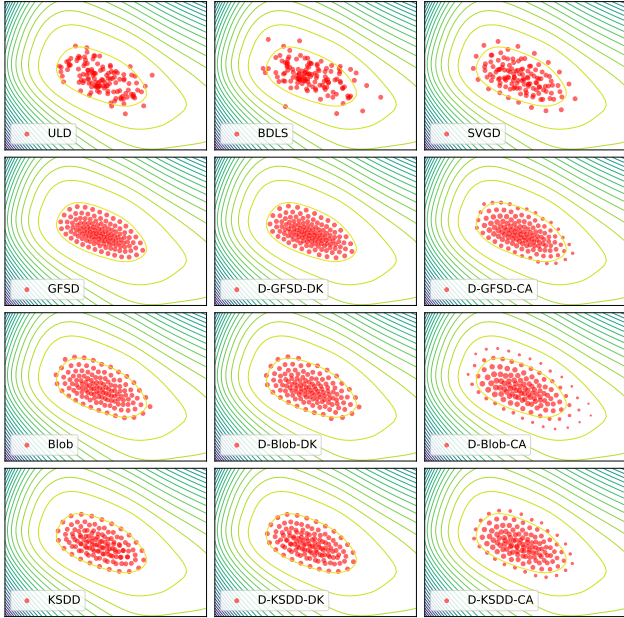


Figure 3: Approximation results in GP with 128 particles.

parameter $\phi = (\phi_1, \phi_2)$ is defined as follows:

$$\log p(\phi|\mathcal{D}) = -\frac{\mathbf{y}^T \mathbf{K}_y^{-1} \mathbf{y}}{2} - \frac{\log \det(\mathbf{K}_y)}{2} - \log(1 + \mathbf{x}^T \mathbf{x}).$$

Here, \mathbf{K}_y is a covariance function $\mathbf{K}_y = \mathbf{K} + 0.04\mathbf{I}$ with $\mathbf{K}_{i,j} = \exp(\phi_1) \exp(-\exp(\phi_2)(x_i - x_j)^2)$ and \mathbf{I} represents the identity matrix. In this task, we set the particle number to $M = 128$ for all the algorithms.

Figure 3 gives the contour line of $\log p(\phi|\mathcal{D})$, and particles generated by each algorithm. It is shown that DPVI algorithms with CA achieve better approximation results compared to other algorithms. We can also observe that D-Blob-CA has the best performance and covers a wider range of area due to both the dynamic weight adjustment strategy and extra repulsive term. We note that the DK strategy barely brings any benefits as there is only one mode in this task and both ParVI with fixed-weight and the DK variants of DPVI spread the equally-weighted particles out over this mode. Actually, the DK variants perform even worse than their fixed-weight ParVI counterparts, since the duplicate/kill operation induces extra fluctuations in this single-mode model.

To evaluate how well the particles approximate the posterior $p(\phi|\mathcal{D})$, we consider two metrics related with the approximation quality. Specifically, we report the W_2 distance and KSD between the empirical distribution and the target distribution in Table 2, given 10000 reference particles generated by the ‘‘gold standard’’ HMC method (Brooks et al. 2011). The result demonstrates the effectiveness of our proposed CA weight strategy: DPVI algorithms with CA constantly outperform their fixed-weight counterparts, and the D-Blob-CA algorithm achieves the highest approximation accuracy among all the algorithms.

Algorithm	Metrics	
	W_2 distance	KSD
ULD	2.365E-1	6.838E-2
BDLS	2.300E-1	6.177E-2
SVGD	1.471E-1	6.200E-4
GFSD	2.096E-1	5.358E-2
D-GFSD-DK	2.124E-1	5.498E-2
D-GFSD-CA	1.569E-1	2.510E-2
Blob	1.494E-1	3.311E-3
D-Blob-DK	1.528E-1	3.926E-3
D-Blob-CA	1.195E-1	5.095E-4
KSDD	1.837E-1	1.279E-2
D-KSDD-DK	1.859E-1	1.367E-2
D-KSDD-CA	1.496E-1	4.659E-3

Table 2: W_2 distance and KSD in GP task.

Algorithm	Datasets			
	Electrical	Concrete	Kin8nm	WineRed
ULD	8.392E+0	6.310E+0	7.857E-2	6.455E-1
BDLS	8.378E+0	6.310E+0	7.843E-2	6.452E-1
SVGD	8.717E+0	6.189E+0	8.044E-2	6.403E-1
GFSD	8.285E+0	6.182E+0	7.880E-2	6.384E-1
D-GFSD-DK	8.226E+0	6.179E+0	7.866E-2	6.384E-1
D-GFSD-CA	8.058E+0	6.173E+0	7.832E-2	6.374E-1
Blob	8.286E+0	6.181E+0	7.880E-2	6.384E-1
D-Blob-DK	8.226E+0	6.178E+0	7.866E-2	6.384E-1
D-Blob-CA	8.058E+0	6.171E+0	7.834E-2	6.374E-1

Table 3: Averaged Test RMSE.

4.3 Bayesian Neural Network

In this experiment, we study a Bayesian regression task with Bayesian neural network on 4 datasets from UCI² and LIB-SVM³. We follow the experiment setting from (Liu and Wang 2016), which models the output as a Gaussian distribution and uses a Gamma(1, 0.1) prior for the inverse covariance. We use a one-hidden-layer neural network with 50 hidden units and maintain 128 particles. For all the datasets, we set the batchsize as 128. Since KSDD-type algorithms require evaluating the Hessian matrix of the objective function, which will induce enormous computational burden in neural network based tasks, we exclude them in this task.

We report the Root Mean Squared Error (RMSE) of each algorithm in Table 3. The results show that both the CA and DK weight strategies contribute to a lower RMSE, and DPVI algorithms with CA achieve the best performance. It can be observed that GFSD-type algorithms obtain similar results as Blob-type algorithms, which may be ascribed to the negative correlation between the magnitude of the repulsive force and the dimensionality in ParVIs (Zhuo et al. 2018).

5 Conclusion

In this paper, we propose a general Dynamic-weight Particle-based Variational Inference (DPVI) framework, which maintains a set of weighted particles to approximate a given target distribution π and updates both the particles’ positions and weights iteratively. Our DPVI framework is

²<http://archive.ics.uci.edu/ml/datasets.php>

³<https://www.csie.ntu.edu.tw/~cjlin/libsvmtools/datasets/>

developed by discretizing a novel composite flow, which is a combination of a finite-particle approximation of a reaction flow and the finite-particle position transport approximation adopted in existing fixed-weight ParVIs. We show that the mean-field limit of the proposed composite flow is actually the gradient flow of certain dissimilarity functional \mathcal{F} in the Wasserstein-Fisher-Rao space, which leads to a faster decrease of \mathcal{F} than the Wasserstein gradient flow underlying existing fixed-weight ParVIs. We provide three effective DPVI algorithms with different finite-particle approximations (D-GFSD-CA, D-Blob-CA, and D-KSDD-CA) and derive three variants of them by using the duplicate/kill strategy. The empirical results show that the proposed DPVI algorithms constantly outperform their fixed-weight counterparts, and D-Blob-CA usually obtains the best performance.

References

- Ambrosio, L.; Gigli, N.; and Savaré, G. 2008. *Gradient flows: in metric spaces and in the space of probability measures*. Springer Science & Business Media.
- Brooks, S.; Gelman, A.; Jones, G.; and Meng, X.-L. 2011. *Handbook of markov chain monte carlo*. CRC press.
- Butcher, J. C. 1964. Implicit runge-kutta processes. *Mathematics of Computation*, 18(85): 50–64.
- Chen, C.; and Zhang, R. 2017. Particle optimization in stochastic gradient mcmc. *arXiv preprint arXiv:1711.10927*.
- Chen, C.; Zhang, R.; Wang, W.; Li, B.; and Chen, L. 2018a. A unified particle-optimization framework for scalable Bayesian sampling. *arXiv preprint arXiv:1805.11659*.
- Chen, W. Y.; Mackey, L.; Gorham, J.; Briol, F.-X.; and Oates, C. 2018b. Stein points. In *International Conference on Machine Learning*, 844–853. PMLR.
- Craig, K.; and Bertozzi, A. 2016. A blob method for the aggregation equation. *Mathematics of computation*, 85(300): 1681–1717.
- Flamary, R.; Courty, N.; Gramfort, A.; Alaya, M. Z.; Boisbunon, A.; Chambon, S.; Chapel, L.; Corenflos, A.; Fatras, K.; Fournier, N.; Gautheron, L.; Gayraud, N. T.; Janati, H.; Rakotomamonjy, A.; Redko, I.; Rolet, A.; Schutz, A.; Seguy, V.; Sutherland, D. J.; Tavenard, R.; Tong, A.; and Vayer, T. 2021. POT: Python Optimal Transport. *Journal of Machine Learning Research*, 22(78): 1–8.
- Gallouët, T.; Laborde, M.; and Monsaingeon, L. 2019. An unbalanced optimal transport splitting scheme for general advection-reaction-diffusion problems. *ESAIM: Control, Optimisation and Calculus of Variations*, 25: 8.
- Gallouët, T. O.; and Monsaingeon, L. 2017. A JKO Splitting Scheme for Kantorovich–Fisher–Rao Gradient Flows. *SIAM Journal on Mathematical Analysis*, 49(2): 1100–1130.
- Jordan, R.; Kinderlehrer, D.; and Otto, F. 1998. The variational formulation of the Fokker–Planck equation. *SIAM journal on mathematical analysis*, 29(1): 1–17.
- Kakutani, S. 1948. On equivalence of infinite product measures. *Annals of Mathematics*, 214–224.
- Kondratyev, S.; Monsaingeon, L.; Vorotnikov, D.; et al. 2016. A new optimal transport distance on the space of finite Radon measures. *Advances in Differential Equations*, 21(11/12): 1117–1164.
- Korba, A.; Aubin-Frankowski, P.-C.; Majewski, S.; and Ablin, P. 2021. Kernel Stein Discrepancy Descent. *arXiv preprint arXiv:2105.09994*.
- Korba, A.; Salim, A.; Arbel, M.; Luise, G.; and Gretton, A. 2020. A non-asymptotic analysis for Stein variational gradient descent. *Advances in Neural Information Processing Systems*, 33.
- Liero, M.; Mielke, A.; and Savaré, G. 2016. Optimal transport in competition with reaction: The Hellinger–Kantorovich distance and geodesic curves. *SIAM Journal on Mathematical Analysis*, 48(4): 2869–2911.
- Liu, C.; and Zhu, J. 2018. Riemannian Stein variational gradient descent for Bayesian inference. In *Proceedings of the AAAI Conference on Artificial Intelligence*, volume 32.
- Liu, C.; Zhuo, J.; Cheng, P.; Zhang, R.; and Zhu, J. 2019. Understanding and accelerating particle-based variational inference. In *International Conference on Machine Learning*, 4082–4092. PMLR.
- Liu, C.; Zhuo, J.; and Zhu, J. 2019. Understanding mcmc dynamics as flows on the wasserstein space. In *International Conference on Machine Learning*, 4093–4103. PMLR.
- Liu, Q. 2017. Stein variational gradient descent as gradient flow. *arXiv preprint arXiv:1704.07520*.
- Liu, Q.; Lee, J.; and Jordan, M. 2016. A kernelized Stein discrepancy for goodness-of-fit tests. In *International conference on machine learning*, 276–284. PMLR.
- Liu, Q.; and Wang, D. 2016. Stein variational gradient descent: A general purpose bayesian inference algorithm. *arXiv preprint arXiv:1608.04471*.
- Liu, Q.; and Wang, D. 2018. Stein variational gradient descent as moment matching. *arXiv preprint arXiv:1810.11693*.
- Lu, Y.; Lu, J.; and Nolen, J. 2019. Accelerating langevin sampling with birth-death. *arXiv preprint arXiv:1905.09863*.
- Ma, Y.-A.; Chen, T.; and Fox, E. B. 2015. A complete recipe for stochastic gradient MCMC. *arXiv preprint arXiv:1506.04696*.
- Mroueh, Y.; and Rigotti, M. 2020. Unbalanced Sobolev Descent. *Advances in Neural Information Processing Systems*, 33.
- Nikulin, M. S.; et al. 2001. Hellinger distance. *Encyclopedia of mathematics*, 78.
- Platen, E.; and Bruti-Liberati, N. 2010. *Numerical solution of stochastic differential equations with jumps in finance*, volume 64. Springer Science & Business Media.
- Pu, Y.; Gan, Z.; Henao, R.; Li, C.; Han, S.; and Carin, L. 2017. VAE Learning via Stein Variational Gradient Descent. In *NIPS*.
- Ranganath, R.; Gerrish, S.; and Blei, D. 2014. Black box variational inference. In *Artificial intelligence and statistics*, 814–822. PMLR.

- Rao, C. 1945. Information and accuracy attainable in the estimation of statistical parameters. Kotz S & Johnson NL (eds.), *Breakthroughs in Statistics Volume I: Foundations and Basic Theory*, 235–248.
- Rasmussen, C. E. 2003. Gaussian processes in machine learning. In *Summer school on machine learning*, 63–71. Springer.
- Rotskoff, G.; Jelassi, S.; Bruna, J.; and Vanden-Eijnden, E. 2019. Global convergence of neuron birth-death dynamics. *arXiv preprint arXiv:1902.01843*.
- Santambrogio, F. 2017. {Euclidean, metric, and Wasserstein} gradient flows: an overview. *Bulletin of Mathematical Sciences*, 7(1): 87–154.
- Süli, E.; and Mayers, D. F. 2003. *An introduction to numerical analysis*. Cambridge university press.
- Wang, Y.; and Li, W. 2019. Accelerated information gradient flow. *arXiv preprint arXiv:1909.02102*.
- Wibisono, A. 2018. Sampling as optimization in the space of measures: The Langevin dynamics as a composite optimization problem. In *Conference on Learning Theory*, 2093–3027. PMLR.
- Zhang, J.; Zhang, R.; Carin, L.; and Chen, C. 2020. Stochastic particle-optimization sampling and the non-asymptotic convergence theory. In *International Conference on Artificial Intelligence and Statistics*, 1877–1887. PMLR.
- Zhang, J.; Zhao, Y.; and Chen, C. 2020. Variance reduction in stochastic particle-optimization sampling. In *International Conference on Machine Learning*, 11307–11316. PMLR.
- Zhu, M.; Liu, C.; and Zhu, J. 2020. Variance Reduction and Quasi-Newton for Particle-Based Variational Inference. In *International Conference on Machine Learning*, 11576–11587. PMLR.
- Zhuo, J.; Liu, C.; Shi, J.; Zhu, J.; Chen, N.; and Zhang, B. 2018. Message passing Stein variational gradient descent. In *International Conference on Machine Learning*, 6018–6027. PMLR.